JOURNAL OF SPACECRAFT AND ROCKETS
Vol. 29, No. 6, November-December 1992

Engineering Method for Calculating Surface Pressures and Heating Rates on Vehicles with Embedded Shocks

D. Brian Landrum* and Fred R. DeJarnette†
North Carolina State University, Raleigh, North Carolina 27695
and
Bret L. Boman‡
McDonnell Aircraft Company, St. Louis, Missouri 63166

An engineering method is described that includes embedded shock waves in three-dimensional surface pressure and heat transfer calculations. Embedded shocks are determined to exist in the flow based on the surface pressure change across discontinuities in the vehicle geometry and oblique shock wave relations. Maslen's approximate technique is used to obtain flowfield properties ahead of the embedded shock. Surface pressures downstream of the shock are calculated by a new Embedded Newtonian pressure method. The importance of accurately modeling the surface geometry, including discontinuities, is discussed and the ASTUD, QUICK, and spline techniques are compared. Code predictions of pressures and heating rates are compared with experimental data for a generic hypersonic vehicle design. In general the comparison is good, especially considering the complexities of the geometries modeled and the approximate nature of the method. Also a substantial reduction in solution time and user interaction in comparison with more exact CFD techniques is discussed. These advantages make the approximate method a useful tool in a preliminary design environment.

Nomenclature

L	= reference body length, ft
M	= Mach number
P	= pressure, lb/in^2
q	= heat transfer rate, Btu/ft^2/s
r	= radial coordinate, ft
T	= temperature, °R
U	= velocity, ft/s
x,y,z	= Cartesian body coordinates
α	= angle of attack, deg
β	= embedded shock angle, deg
Γ	= bow shock wave angle, deg
γ	= ratio of specific heats
ρ	= mass density, slug/ft^3
Φ	= circumferential body angle, deg
Ψ	= stream function
ψ	= angle between surface unit normal and freestream velocity vector, deg

Subscripts

B	= body
e	= edge of boundary layer
emb	= embedded shock
REF	= reference plane
s	= stagnation condition
shk	= shock wave
w	= wall
∞	= freestream condition
1	= ahead of embedded shock
2	= aft of embedded shock

Received Nov. 27, 1991; presented as Paper 91-5060 at the AIAA 3rd International Aerospace Planes Conference, Orlando, FL, Dec. 3-5, 1991; revision received March 4, 1992; accepted for publication March 5, 1992.

*Research Assistant, Mechanical and Aerospace Engineering. Member AIAA

†Professor, Mechanical and Aerospace Engineering. Associate Fellow AIAA

‡Lead Engineer, Propulsion and Thermodynamics; currently Senior Engineer, B & W Nuclear Technologies, Lynchburg, VA 24506. Senior Member AIAA.

Introduction

THE development of aerospace planes has created a resurgence of research into hypersonic flows. This revival requires improved tools to optimally design and analyze new vehicle concepts. Parameters such as surface pressures, forces and moments, and heating rates must be accurately predicted.

Progress has been made in computing viscous, compressible flow over increasingly complex vehicles by solving the full Navier-Stokes equations or some simplified form such as the viscous shock layer (VSL) or parabolized Navier-Stokes (PNS) equations. But, in general, these methods are too costly in terms of effort required for input parameters, computational time, and storage for extensive design calculations. Classical approaches such as the inviscid/boundary-layer methods may also prove to be too computationally intensive. Thus there is a continuing need for approximate techniques that can efficiently analyze candidate vehicle configurations over a wide range of flow regimes and geometry parameters.

A simple method for computing the three-dimensional boundary-layer flow over a vehicle is the "axisymmetric analog" method developed by Cooke.[1] In this approach the three-dimensional boundary-layer equations are written in a streamline coordinate system, and the crossflow velocity is assumed to be zero. The three-dimensional boundary-layer equations reduce to a form that is identical to those for axisymmetric flow provided that 1) the distance along a streamline is interpreted as the distance along an "equivalent" axisymmetric body and 2) the metric coefficient that describes spreading of the streamlines is interpreted as the radius of the equivalent body. Thus, in regions where the small crossflow assumption is valid, any existing axisymmetric boundary-layer program can be used to compute the approximate three-dimensional heating along a streamline. By considering multiple streamline paths, the entire vehicle of interest can be covered. This technique was refined by DeJarnette,[2] who along with Hamilton later modified the method to include the effects of entropy layer swallowing.[3] Various manifestations of what is herein called the DeJarnette heating code are currently used in codes such as the Air Force AERHET[4] and STAPAT[5,6] codes, and other codes used by NASA and industry.

A critical requirement for applying the axisymmetric analog technique is accurate computation of the inviscid surface streamline paths and the metric coefficients associated with

streamline spreading. Definition of the streamlines and metrics is directly dependent on an adequate description of the vehicle geometry, including body radius, slope, and curvature in the axial and circumferential directions. Many of the new hypersonic vehicle concepts under consideration include surface discontinuities such as compression ramps ahead of engine inlets, fuselage/canopy junctures, and control surfaces. At high speeds, shock waves may form at these discontinuities. Formation of these embedded shocks results in a surface pressure rise and hence an increase in heat transfer rates that could have a major design impact. Techniques to model the effects of embedded shocks on heat transfer have been developed previously.[7,8] These methods were applied in an inviscid/boundary-layer approach that requires a significant amount of computation to determine the inviscid flowfield properties. Also, to adequately capture embedded shocks, substantial grid refinement is often required. Calculation of the embedded shocks in an approximate technique can reduce this time investment.

This paper first contrasts and compares several readily available techniques for analytically describing vehicle surface geometry. Issues of interest include model development time and complexity, model accuracy in relation to geometry representation and flow calculations, and user interaction. Then a method to include embedded shock waves in the prediction of surface pressures and heating rates is developed.

Vehicle Geometry Definition

Surface streamline and metric calculations for approximate heating codes require definition of body radius, slope, and curvature in the axial and circumferential directions for a given body location. The correspondence between surface pressure and geometry in this technique is the result of using the Modified Newtonian pressure method that relates pressure to vehicle surface inclination angle. At zero angle of attack the local surface inclination angle along a centerline is directly related to the axial body slope. Several readily available techniques for modeling vehicle surface geometry exist. The choice of the technique to be employed depends on flowfield analysis tool requirements, vehicle complexity, model development time, desired accuracy, etc.

Cheatwood et al.[9] reviewed and critiqued existing geometry modeling techniques in their paper describing the advanced surface-fitting technique featuring user-friendly development (ASTUD) geometry modeler. In their summary, panel methods were described as having problems with interpanel discontinuities and storage of numerous, difficult-to-obtain geometry values. Spline methods are plagued by undesirable wiggles, dimples, or bulges in the resulting model. However, spline techniques can be easily incorporated into flowfield analysis codes and do not require a separate model development effort

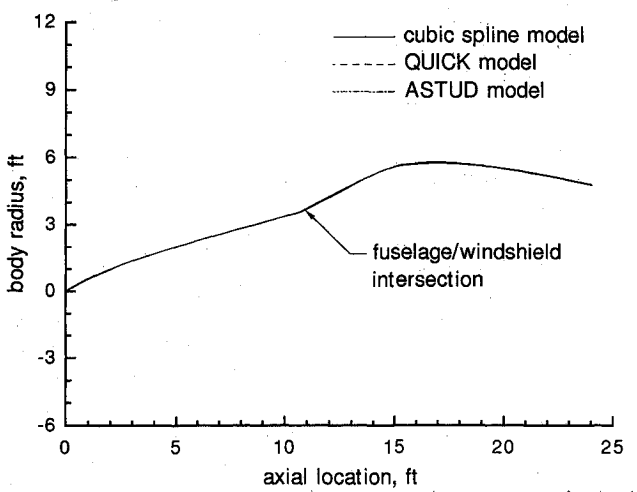

Fig. 1 Comparison of body radius variation along top centerline of an F-15 like forebody.

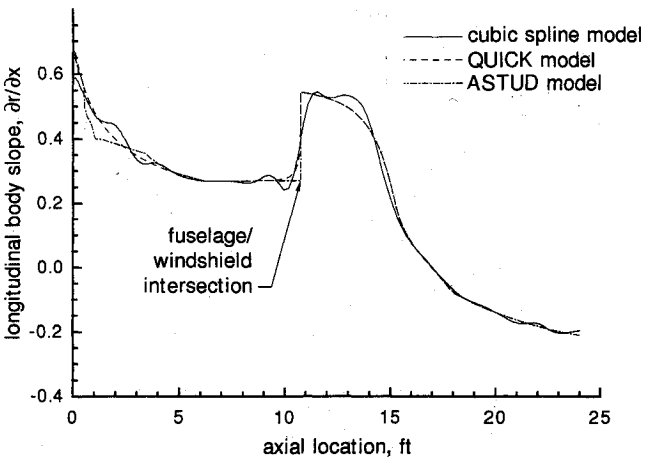

Fig. 2 Comparison of longitudinal body slopes along the top centerline of an F-15 like forebody.

in which the user fits the input cross-sectional body points. The QUICK[10] technique is believed to provide accurate results but requires large initial set up times. Since the Cheatwood review, however, QUICK has been improved[11] in terms of user friendliness for model development.

Both ASTUD and QUICK are stand-alone programs that require cross-sectional data point files as input. After fitting the points, the user may review and alter the fits. Both programs also provide FORTRAN subroutines to interrogate the resulting output files to yield the required parameters for streamline calculations.

With ASTUD the user first fits the cross-sectional data points with a general conic or straight line between control points. Initially, the top and bottom centerline data points are designated control points. Additional control points (which may or may not coincide with data points) can be designated. This allows several conic sections to be employed to improve the accuracy of the fit. At control points, adjoining conic section slopes can be specified as either continuous or discontinuous. Through interactive graphics the strategic placement or removal of control points to produce the optimum fit of the cross-sectional data is greatly facilitated.

After all cross sections are fit, the nose region is modeled. The nose radius is either user defined (using elliptical or spherical options) or computed automatically from two user-specified cross sections. This fit can also be reviewed and altered as desired.

Finally, the body is fitted longitudinally using an approach similar to the cross-sectional fitting. Longitudinal data points are formed by intersecting meridional cuts (spaced at 3.6-deg increments) with the fitted cross sections. Default control points are defined at the end of the nose region and the end of the body. Intermediate control points can then be added to improve the conic section fit to the data points.

For the QUICK model, as with ASTUD, the body is fit cross sectionally and then longitudinally. In QUICK, however, the user can fit the cross sections with straight lines, ellipses, circular arcs, and conic loft segments. Control points begin and end each segment. In addition, a third point, known as the slope point, is specified to control the shape of the segment. These control and slope points must be chosen judiciously because they must be fit longitudinally. The vehicle can be broken up into several longitudinal regions or models in which the relative positions of the control and slope points remain constant. These models are then connected by linking and blending the control and slope points. It is this longitudinal fitting that requires good model preplanning and bookkeeping to assure a successful model.

To aid in choosing a geometry modeling technique, three methods (ASTUD, QUICK, and spline functions) are compared in their respective descriptions of an aircraft forebody

and canopy system similar to that of the F-15. Each resulting model is then used in the newest version of the STAPAT[6] code (which employs the approximate heating code of DeJarnette) to demonstrate its utility in calculating surface pressures and heating rates.

The top centerline radii as fit by each method are compared in Fig. 1. All three methods agree well, although the cubic spline values are slightly lower because the body radii are smoothed after being fitted. The major differences in the three techniques are shown in Fig. 2 where the local body slope, $\partial r/\partial x$, is shown as a function of axial location. In regions where the surface geometry is continuous, all three modeling techniques provide consistent slope values. The results differ, however, in areas of discontinuity (e.g., the fuselage/windshield junction). QUICK and ASTUD correctly model the intersection by a sudden change in axial body slope. The cubic spline method rounds this discontinuity and produces wiggles in this region. Rounding the corner significantly affects the predicted location of peak pressures and heating rates as will be shown. The somewhat erratic slope values shown for the ASTUD model near the nose are due to an inadequate implementation of the technique and are not representative of its capabilities.

Using these geometry definitions, the heating code was then used to predict surface pressures and heating rates over the aircraft forebody of Figs. 1 and 2. Surface pressure and turbulent heat transfer comparisons along the top centerline are shown in Figs. 3 and 4. Again, all three methods are comparable except near the fuselage/windshield intersection. In this region, QUICK and ASTUD predict a sudden increase in pressure and heating rate, as expected. The cubic spline method exhibits the effects of corner rounding and wiggles, and peak pressure is incorrectly predicted downstream of the intersection.

In modeling surfaces where discontinuities typically exist, use of QUICK or ASTUD is recommended, though the cubic spline method may provide acceptable results, depending on the accuracy required. From our experience, modeling with ASTUD is easier than QUICK, although QUICK has some advantages in file management. The three modeling techniques are compared in Table 1 from Ref. 6. A more detailed comparison of the three techniques can also be found in Ref. 6.

Streamline Integration in the Nose Region

In a previous version of the DeJarnette heating code,[5] a cross-sectional starting plane is chosen (designated XZERO) along with an initial distribution of circumferential angles Φs. This choice is to guarantee an adequate coverage of the body with streamlines for heat transfer calculation. Ahead of this plane, the body was assumed to be represented by a sharp

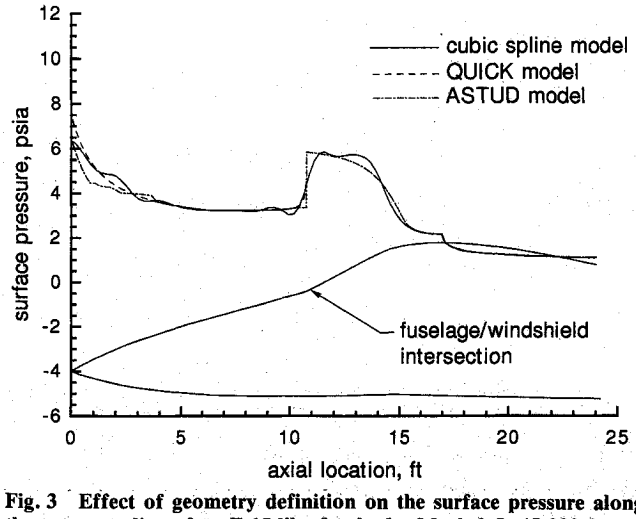

Fig. 3 Effect of geometry definition on the surface pressure along the top centerline of an F-15 like forebody, Mach 2.5, 45,000 ft.

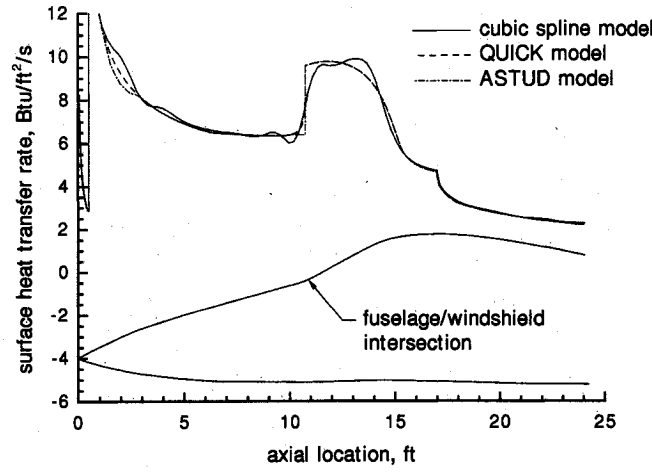

Fig. 4 Effect of geometry definition on the surface heating rate along the top centerline of an F-15 like forebody, Mach 2.5, 45,000 ft.

cone. Analytic solutions were generated based on this cone to begin streamline integration downstream. For truly blunt-nosed bodies this representation is inadequate and the approach has been modified to allow for either a blunt or sharp nose.

A problem with the blunt nose is that the initial location of the streamline near the stagnation point that will pass through the desired point at XZERO is unknown. A new approach has been developed that traces the streamline from XZERO forward to determine this initial location near the stagnation point. Streamlines are integrated from the point (XZERO,Φ) toward the stagnation region by a fourth-order, constant step size Runge-Kutta integration routine. The detailed equations for streamline calculation are derived in Ref. 2. During the forward integration, more accurate results can be obtained by using Cartesian body coordinates (x,y,z) of the streamline. Streamline direction is determined by the so-called method of steepest descent and is only a function of body geometry and vehicle angle of attack. These streamlines are also referred to as simplified or Newtonian.

Near the stagnation point analytical solutions derived in Ref. 3 are used to obtain starting values for the metric and other parameters associated with the heat transfer calculations. Currently, the DeJarnette heating code utilizes the locally similar boundary-layer equations of Refs. 12–14 to obtain the ratio of local heating rate to the stagnation point value $(q_w/q_{w,s})$. These analytical starting values are based on the shock standoff distance and shock radii of curvature at the stagnation point, which are also calculated in the code. The streamline coordinates are then reintegrated along with the metric and heat transfer integral back to the starting point (XZERO) for the downstream streamline integration to commence. Calculations from XZERO downstream can be based on a laminar, turbulent, or transitional boundary layer when the transition region is specified.

Calculation of Embedded Shocks

Existing engineering codes are not capable of calculating heating rates over vehicles with embedded shock waves. These shocks are formed by ramps, windshields, or other geometry features that require a compressive turning of the flow. A new method is developed here to calculate heating rates over these vehicles. It was found that Modified Newtonian pressures were not accurate enough for the heating calculations. Therefore a new Embedded Newtonian technique is developed to predict the pressure distribution downstream of embedded shocks.

The embedded shock calculations can best be described by considering Fig. 5. This figure illustrates a centerline streamline, but the method is identical for other streamlines. When

Table 1 Summary of geometry fitting techniques

Model Aspect	Cubic spline	ASTUD	QUICK
Automation	Complete	Nearly complete, little extra work involved, all menu driven	Minimal, user must keep track of control point, body line names, and curves completed, mostly menu driven
File management	Input is simply a cross-section data point file	Awkward, files named by unit number, difficult to keep track of progress	Easy with direct access files, all under one case name with different specifiers
Setup time	none	Minimal, program very automated	Long, user must plan control point location and name on all cross sections
Ease of modeling	NA	Easy modeling, automatic sequential modeling process	Diffucult, body line concept complex and prone to error
Length of modeling process	NA	Long, fitting of 51 longitudinal fits is tiring	Depending on good planning, the number of body lines to model can be minimized
Modeling error checking	NA	If errors in slope or curvature exist, the user is notified	Few error prompts for piecing curves exist
Nose region fit	Currently limited to sharp cones only	Good flexibility and options: constant radius with respect to Φ, ellipse, or determined by program	Fit with body lines
Discontinuity modeling	Discontinuities are rounded	Good sharp breaks	Good sharp breaks
Viewing capabilities	None	Zoom, orthographic, cross section, longitudinal, and original data comparison	Same as ASTUD
Restart feature	NA	Awkward, must rename files, many places to terminate	Good, eased by main executable, good file management scheme
CPU/CPU_{min}	1.0	1.5	1.8
Accuracy of radius	Average, worse with smoothing functions	Very good	Very good
Reasonableness of derivatives	Smoothing changes geometry, forces derivatives to look good	Deviations can become magnified	Deviations can become magnified

variable boundary-layer edge entropy effects are included in the calculations, the bow shock angle (Γ_{shk}) above each integrated streamline point is determined by a modification of Maslen's pressure technique[15] as described in Ref. 3. The values of pressure and stream function at the shock (P_{shk} and Ψ_{shk}) are also calculated by this modified method. The body pressure (P_B) is determined by the modified Newtonian pressure equation

$$\frac{P_B}{P_s} = \left(1 - \frac{P_\infty}{P_s}\right)\cos^2\psi + \frac{P_\infty}{P_s} \tag{1}$$

where the angle ψ is the angle between the surface unit normal and the freestream velocity vector, and P_s and P_∞ are the freestream stagnation and static pressures, respectively. The stream function on the body Ψ_B is defined as identically zero.

The boundary-layer edge stream function for each body point Ψ_e can be obtained by a local mass flux balancing in the shock layer.[3] With values for Ψ_e, Ψ_{shk}, P_{shk}, and P_B determined, Maslen's pressure technique[15] can then be used to obtain the boundary-layer edge pressure by

$$P_e = P_{shk} - (PFACT)(\Psi_e - \Psi_{shk}) \tag{2}$$

where

$$PFACT = \frac{(P_B - P_{shk})}{\Psi_{shk}} \tag{3}$$

Other important properties such as U_e, ρ_e, and M_e are also calculated by this method.

Now consider an axial point x_1 ahead of a surface discontinuity such as a ramp and a point x_2 on the ramp as shown in Fig. 5. If the body slope at the second point $(\partial r/\partial x)_2$ is greater than the preceding body slope $(\partial r/\partial x)_1$, as is the case in this example, then an embedded shock can potentially exist. The criteria for the existence of an embedded shock is based on the ratio of the modified Newtonian surface pressures (P_{B_2}/P_{B_1})

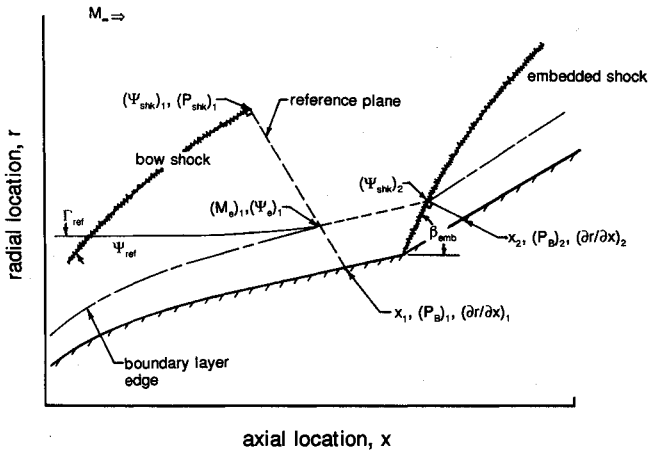

Fig. 5 Illustration of the embedded shock methodology.

and the two-dimensional shock relations for a perfect gas.[16] Rewriting the static pressure relation for an oblique shock shows that the normal component of the preshock Mach number is

$$M_{1_n} = M_1 \sin \beta_{\text{emb}} = \sqrt{\frac{(\gamma+1)(P_{B_2}/P_{B_1}) + (\gamma-1)}{2\gamma}} \tag{4}$$

A measure of shock strength is the entropy increase across the shock that is proportional to $(M_{1_n}^2 - 1)^3$ (see Ref. 17). The increase is not considered important to our flow calculations unless $M_{1_n} \geq 1.3$. When M_{1_n} meets the minimum value an embedded shock is included in the calculations. The preshock Mach number for the ramp point at x_2 is then considered to be the boundary-layer edge Mach number at x_1, i.e., M_{e_1}. The initial embedded shock angle is determined by

$$\sin \beta_{\text{emb}} = \frac{M_{1_n}}{M_{e_1}} \tag{5}$$

Note that this angle is referenced to the freestream velocity, which is consistent with the Modified Newtonian body pressures.

The bow shock is now discontinued and variable entropy calculations are based on the new embedded shock. But the embedded shock slope is determined by the inviscid shock-layer flow ahead of the ramp and not by the freestream flow as was the case for the bow shock. Therefore a "reference" data plane is formed between the body point x_1 and the bow shock above it (see Fig. 5). This plane is divided into 21 stations, including the body where $\Psi_B = 0$. Based on the stream function at the shock, reference plane stream function values are given by

$$\Psi_{\text{REF}_n} = n\Psi_{\text{shk}_1}/20 \tag{6}$$

where $n = 0, 1, 2, \ldots, 20$. The pressure at each station (P_{REF_n}) is determined by replacing Ψ_e with Ψ_{REF_n} in Maslen's Eq. (2). The stream function at each reference plane station also has an associated bow shock angle it has passed through. This angle, designated Γ_{REF_n}, is interpolated from the array of bow shock stream functions and shock angles calculated for all of the previous body stations. As with the original variable entropy calculations, Γ_{REF_n} and P_{REF_n} can then be used to determine other reference plane properties, U_{REF_n}, ρ_{REF_n}, and M_{REF_n} (see Ref. 3).

At the first ramp point x_2, the stream function at the embedded shock is assumed to be the boundary-layer edge stream function at the previous point ($\Psi_{\text{shk}_2} = \Psi_{e_1}$). This allows calculation of P_{shk} at x_2. This shock point is also considered the boundary-layer edge at x_2. As streamline integration proceeds down the body, the embedded shock slopes are now calculated with the modified Maslen's technique just as the bow shock slopes were, but the preshock reference properties replace the freestream properties. The appropriate values of P, U, ρ, and M in the reference plane, for a local Ψ at the embedded shock or boundary-layer edge, are interpolated from the reference plane values. If a point on the embedded shock requires shock-layer properties referenced to a bow shock point that is past termination, then the properties at the point of termination are used. The heating rate calculations for the new embedded shock are made in the same manner as when the bow shock is considered.

When another body slope increase is encountered, such that a second embedded shock is formed, the procedure described earlier is repeated. The first embedded shock is discontinued and a new reference plane is created. Thus, multiple embedded shocks are allowed with this technique. It should also be noted that with this approach, if the surface geometry is not modeled accurately, spurious slope changes can cause formation of a shock where one should not occur.

Surface Pressures with Embedded Shocks

In an effort to improve the surface pressure calculations when embedded shocks are present, a new pressure calculation method was formulated. When an embedded shock is formed, the surface pressures downstream of the shock are calculated by replacing the freestream pressure in the Modified Newtonian Eq.(1) with the body pressure at the station ahead of the shock (P_{B_1} in Fig. 5). The body pressure is then calculated by what in this paper is called the Embedded Newtonian equation

$$\frac{P_{B_2}}{P_s} = \left(1 - \frac{P_{B_1}}{P_s}\right)\cos^2\psi + \frac{P_{B_1}}{P_s} \tag{7}$$

Note that in this equation the stagnation pressure P_s is still the freestream value. Comparisons with data from wind tunnel tests of a generic hypersonic vehicle configuration indicated that this technique is more accurate using freestream stagnation pressure than the local stagnation pressure ahead of the embedded shock.[18] The existence of the first embedded shock is determined by the ratio of the Modified Newtonian body pressures [Eq. (1)] and the Mach number criteria described in the previous section. Successive embedded shocks are determined by the ratio of the Embedded Newtonian body pressures [Eq. (7)] on either side of the ramp and the Mach number criteria. The Embedded Newtonian method is similar in approach to the "variable coefficient" Newtonian calculations described in Ref. 19 in that both methods result in a stagnation pressure coefficient that can exceed the theoretical limit of 2. But the current method is based on analytical calculations and not empirical corrections. This new pressure calculation methodology is discussed further in Ref. 18 and is

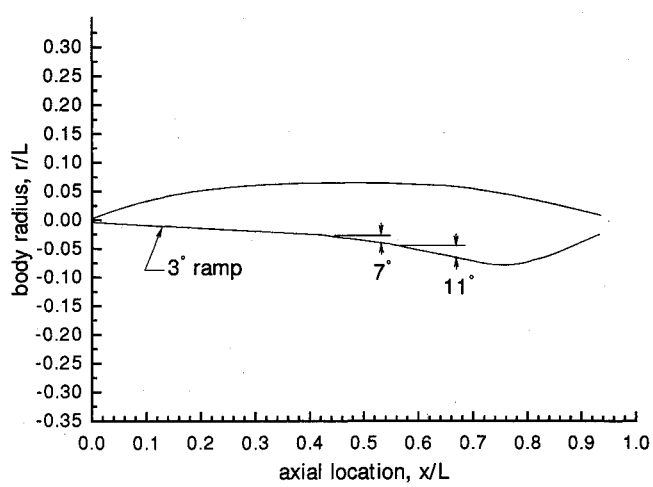

Fig. 6 BWB wind-tunnel model profile as generated by the ASTUD geometry modeling program.

different from the unsteady Embedded Newtonian method of Ericsson.[20]

Results for Complex Flowfield

The following results were obtained by extending the DeJarnette heating code (as formulated in Ref. 5) to include embedded shocks as discussed previously. This modified method was then implemented in the framework of the STAPAT II code.[6] The code was used to analyze the flow about a wind tunnel model of a generic hypersonic configuration that is representative of many vehicles of current interest. This is a McDonnell Douglas design known as the blended wing body configuration. Figures 6 and 7 show profile and orthographic views of the model as generated by ASTUD. The body consists of a smoothly contoured upper surface. The lower surface downstream of the nose is essentially a series of ramps. The forebody has a 3-deg slope followed by 7-deg and 11-deg compression ramps. The aft body section is a boat-tail shaped expansion region. The vehicle model is approximately 3% of full scale. Two spherical noses (one relatively sharp and the other blunt) were fit to the model. The results presented here are for the sharp nose. The model has been tested over a range of angles of attack and Mach numbers. Details of the model geometry and instrumentation may be obtained from Ref. 21. This model is a challenging test of the modified code predictive capabilities in that it includes complex geometric features such as inlet compression ramps and fuselage chines.

The computational representation of the body was generated by the ASTUD geometry modeler[9] for the sharp nose radius. Experimental conditions and resultant data were provided by McDonnell Douglas. The two experimental cases used for comparison to STAPAT II predictions are described in Table 2. For both comparisons the wall to stagnation temperature ratio (T_w/T_s) was set to 0.209. For each case the code was run assuming all laminar flow and then run assuming

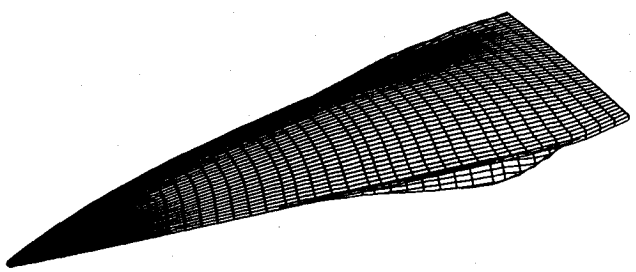

Fig. 7 Orthographic view of the BWB model as generated by the ASTUD geometry modeling program.

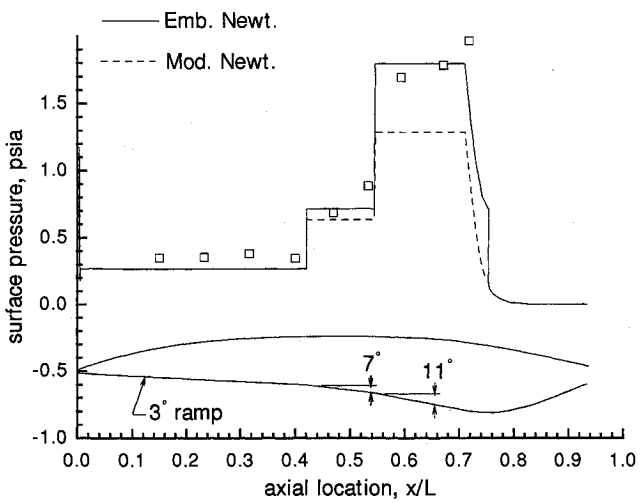

Fig. 8 STAPAT II comparison with pressure data along the bottom centerline of the BWB model, Mach = 11.32, $\alpha = 0$ deg.

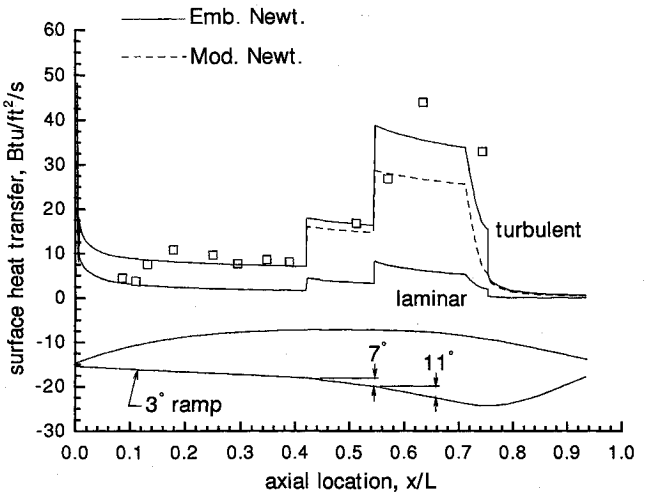

Fig. 9 STAPAT II comparison with heat transfer data along the bottom centerline of the BWB model, Mach = 11.32, $\alpha = 0$ deg.

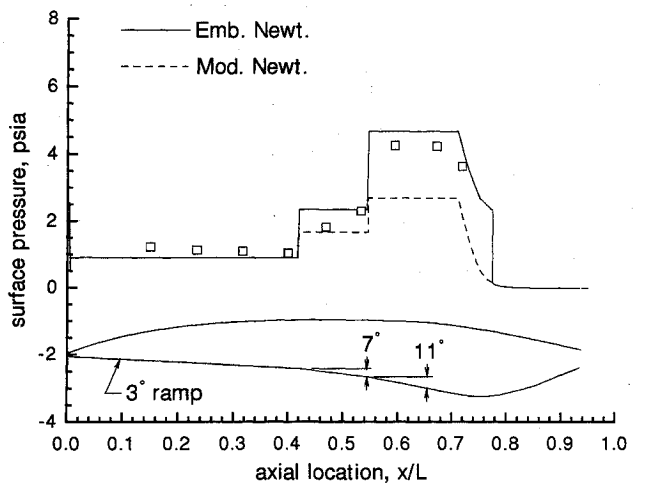

Fig. 10 STAPAT II comparison with pressure data along the bottom centerline of the BWB model, Mach = 11.31, $\alpha = 6$ deg.

transition to turbulent flow close to the nose (at $x/L = 0.02$). A total of 41 streamlines were calculated for each case. All numerical computations were performed on a VAX 8700. A typical run time for the $\alpha = 6$-deg case was 729 s for 41 streamlines or approximately 18 s per streamline.

Plots comparing numerical results and experimental data on the lower centerline are shown in Figs. 8–11. Experimental data are given by the open squares and the numerical calculations are shown by the solid and dashed lines. Results based on the Modified Newtonian method (no embedded shocks) are designated by dashed lines. The solid lines designate results obtained by the new Embedded Newtonian method previously described.

Pressure calculations for $\alpha = 0$ deg are shown in Fig. 8. Since there are no embedded shocks on the forebody, both calculation techniques predict the same surface pressures forward of the first ramp. The experimental forebody pressures are underpredicted by about 25%. The leading data point on the first ramp is nearly matched by both calculations. The second data point is underpredicted by 19%. On the aft ramp the Modified Newtonian pressures are significantly lower than the experimental values. The Embedded Newtonian method on the other hand does quite well, predicting pressure magnitudes to within 9%.

Heat transfer rate comparisons for $\alpha = 0$ deg are shown in Fig. 9. Data indicate transition occurs between $x/L = 0.1$–0.25, and thus the vehicle boundary layer is predominantly turbulent. The computational methods underpredict the fourth and fifth forebody data points by about 20%. This

Table 2 Wind tunnel conditions

	Case 1	Case 2
Mach	11.32	11.31
α, deg	0	6
P_∞, psia	0.1836	0.1790
T_∞, °R	104.7	104.2
T_w, °R	582.9	579.1
Re/ft	9.5×10^6	9.3×10^6

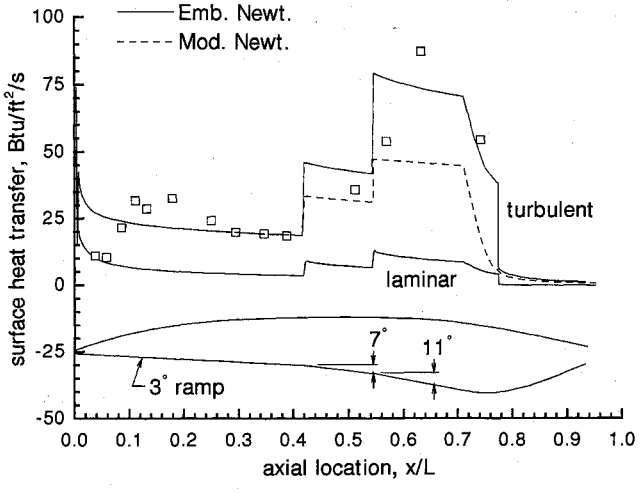

Fig. 11 STAPAT II comparison with heat transfer data along the bottom centerline of the BWB model, Mach = 11.31, $\alpha = 6$ deg.

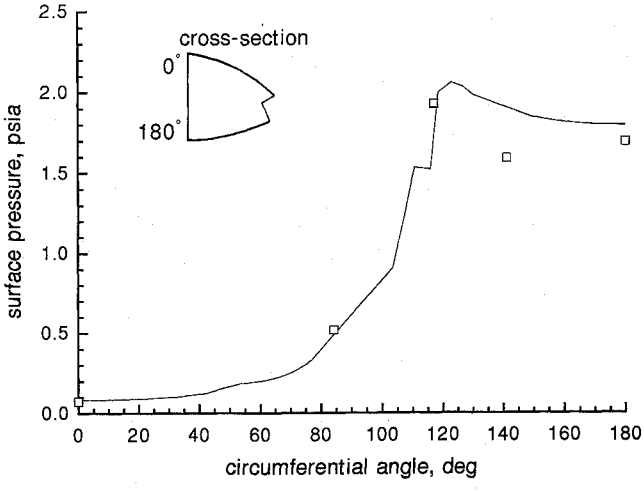

Fig. 12 STAPAT II comparison with circumferential pressure data at $x/L = 0.594$ on the BWB model, Mach = 11.32, $\alpha = 0$ deg.

is not unexpected since the actual transition region was not modeled for this simulation. Near the end of the forebody where fully turbulent flow has been established, the heating rates are accurately predicted. The single data point on the first engine inlet ramp is exactly matched by the Embedded Newtonian method, whereas the heating rates using Modified Newtonian pressures are below this value. Results are mixed on the second ramp. The Modified Newtonian method matches the heat transfer rate at the front of the ramp but significantly underpredicts the heating rate on the rest of the ramp. The Embedded Newtonian method overpredicts the first data point by 40% and underpredicts the second point by 20%, but the method appears to predict the overall heat load on the aft ramp. A possible explanation for this discrepancy is shock wave induced boundary-layer separation on the ramps that the approximate technique does not model. Unfortunately, the sparsity of experimental data on the ramps inhibits a complete understanding of the flowfield and comparisons with the computations.

Pressure comparisons are shown for $\alpha = 6$ deg in Fig. 10. The computed forebody pressures compare favorably with measurements. On the ramps the Modified Newtonian method underpredicts the pressure levels by as much as 35% except for the first data point. The Embedded Newtonian method is more accurate but generally overpredicts the ramp pressures. On the first ramp, the pressure at the first point is computed to be 29% higher than that measured, but the level at the second point is matched exactly. The computation compares much better on the aft ramp where the measured data is predicted to within 10%.

The associated heating rates for $\alpha = 6$ deg are presented in Fig. 11. A large heating peak on the forebody is not captured by either computation, but this again occurs in the transition region that was not modeled. Consistent with the pressure results the Modified Newtonian method underpredicts the heat transfer rates on the ramps. The Embedded Newtonian method predicts an 18% higher heat transfer rate than that measured on the first ramp. As in the $\alpha = 0$-deg case, this method also predicts higher (by 44%) heating rates on the front of the aft ramp but underpredicts the other data points by approximately 15%. The total heat loading on the aft ramp appears to be predicted. Again, the behavior of the ramp heat transfer rates is possibly attributable to boundary-layer separation. But the coarse spatial distribution of the data hinders a resolution of the discrepancies between computation and experiment.

Upper surface centerline comparisons for the sharp nose configuration were also determined, although not shown here. These comparisons exhibited good agreement between the ex-

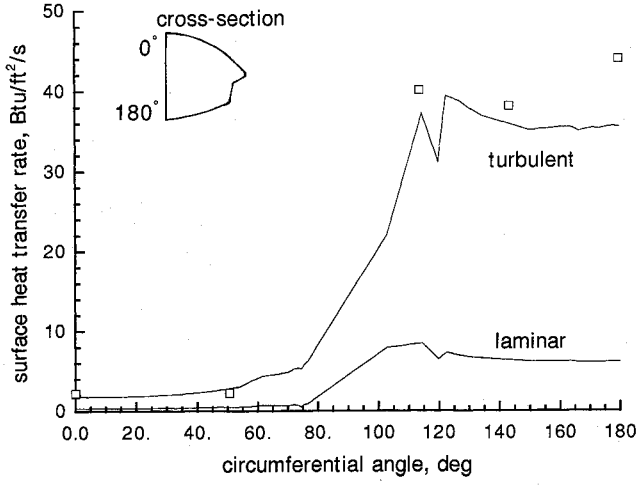

Fig. 13 STAPAT II comparison with circumferential heat transfer data at $x/L = 0.633$ on the BWB model, Mach = 11.32, $\alpha = 0$ deg.

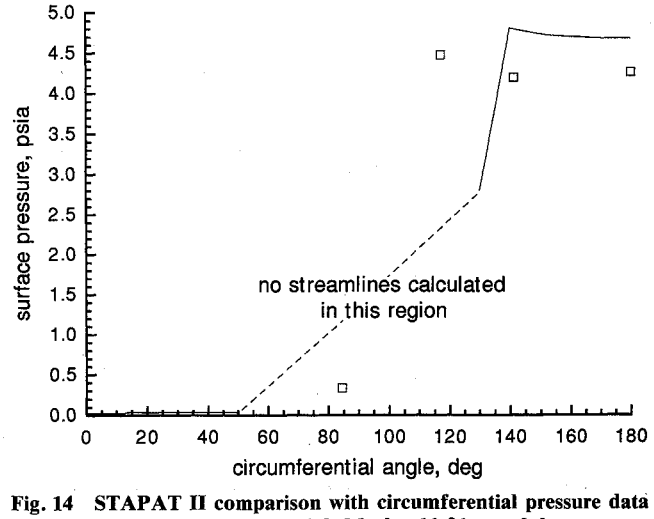

Fig. 14 STAPAT II comparison with circumferential pressure data at $x/L = 0.594$ on the BWB model, Mach = 11.31, $\alpha = 6$ deg.

perimental and predicted pressures and heating rates. The results are discussed in detail in Refs. 6, 19, and 22.

Off-centerline pressure and heat transfer calculations at two axial stations are given in Figs. 12 and 13 for $\alpha = 0$ deg. Only computations using the new Embedded Newtonian method are shown. The comparisons are generally good for pressure and heating rate with the largest deviations of approximately 20% occurring on the windward side of the model. The agreement is reasonable considering the approximate nature of the calculation technique and the complexity of the circumferential geometry modeled.

Figures 14 and 15 show circumferential comparisons for 6-deg angle of attack. A complete comparison between calculations and experiment was not made due to inadequate streamline coverage in the chine region. This problem could be alleviated by a better initial choice of the number and distribution of streamlines. Part of the problem may be attributable to the geometry resolution of the ASTUD technique. The circumferential geometry is fit at 3.6-deg increments. This resolution does not allow the chine to be modeled as a sharp point. This issue was also addressed briefly in a paper by Thompson and Gnoffo[23] in which the same vehicle was modeled by the ASTUD technique. Considering only circumferential stations where streamlines and test data coincide, reasonable agreement with the Embedded Newtonian predictions is shown. Maximum deviations are around 15% for both pressure and heat transfer rate.

The previous comparisons show that the inclusion of embedded shocks significantly improves the predictive capabili-

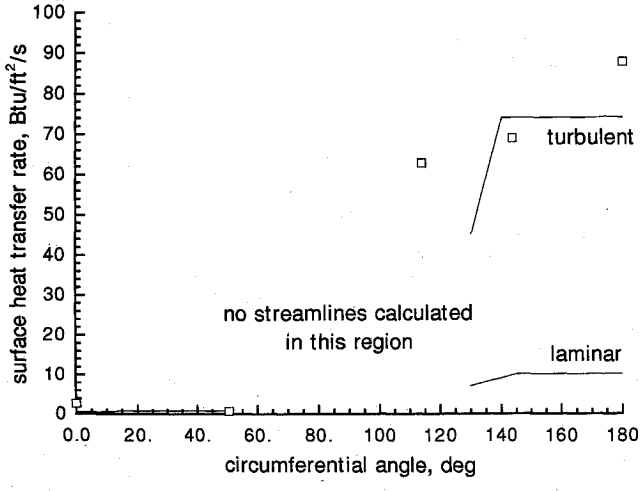

Fig. 15 STAPAT II comparison with circumferential heat transfer data at $x/L = 0.633$ on the BWB model, Mach = 11.31, $\alpha = 6$ deg.

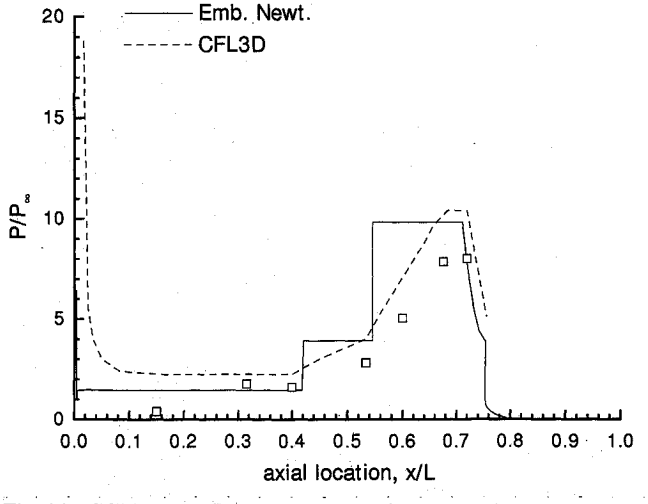

Fig. 16 CFL3D and Embedded Newtonian comparisons with pressure data along the bottom centerline of the BWB model, Mach = 11.35, $\alpha = 0$ deg.

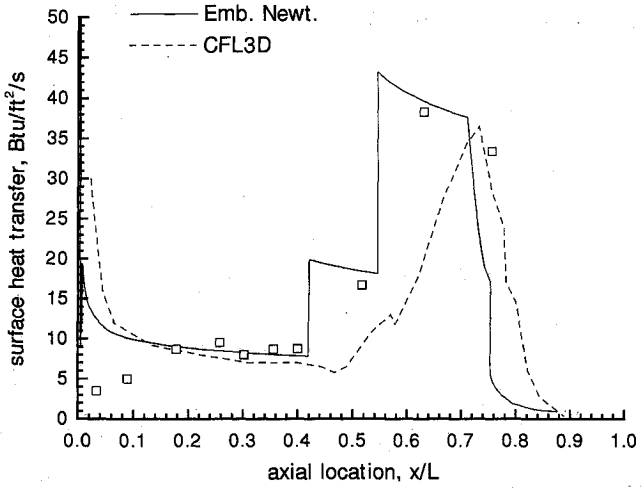

Fig. 17 CFL3D and Embedded Newtonian comparison with turbulent heat transfer data along the bottom centerline of the BWB model, Mach = 11.35, $\alpha = 0$ deg.

ties of engineering design techniques. The approximate Embedded Newtonian method predicts pressures and heating rates on the complex blended wing body (BWB) configuration reasonably well. The accuracy of this new approximate technique can be evaluated further by comparing it with the predictive capabilities of more exact computational fluid dynamics (CFD) methods. The BWB configuration has also been analyzed by several thin-layer Navier-Stokes codes. The LAURA code was used to calculate pressures and laminar heating rates over this geometry.[23] A more detailed comparison was made by Richardson et al.[24] using the CFL3D thin-layer Navier-Stokes code, and some of these results are presented here.

Figure 16 shows experimental and computed pressures on the BWB lower centerline at Mach 11.35 and 0-deg angle of attack. Again, experimental data are indicated by open squares and the Embedded Newtonian calculations by solid lines. The CFL3D results are represented by dashed lines. The low magnitude of the first forebody data point is not predicted by either code. The other forebody data points are overpredicted by the CFL3D code but nearly matched by the approximate technique. Both computational methods overpredict the only data point on the first ramp by 35%. On the aft ramp the CFL3D method predicts a pressure on the front of the ramp that is 40% higher than the measured value. The Embedded Newtonian method predicts an even higher value. The other data points on the aft ramp are overpredicted by the approximate technique by about 25%, but the exact code compares even less favorably.

In Fig. 17 the prediction of heat transfer rates along the lower centerline is shown assuming a fully turbulent boundary layer. The experimental data indicate that transition may extend as far back on the vehicle as $x/L = 0.25$. Beyond $x/L = 0.18$ the forebody heat transfer rate is predicted within 10% by the Embedded Newtonian method. The exact method does not compare as well. The CFL3D code significantly underpredicts the heating rates on the ramps with maximum deviations as high as 45%. In contrast, the approximate technique does much better, generally predicting the ramp heat transfer within 10%. This poor prediction of the ramp heating rates by the exact method may be due to inadequate grid resolution. A grid refinement study was performed as discussed in Ref. 24, but further refinement would possibly decrease the discrepancy between the computation and the measurements. Computing times for the CFL3D results are not known. Similar laminar results obtained by the LAURA code in Ref. 23 required approximately 6.5 h on a Cray-2S supercomputer. However, this value does not reflect any multitasking or parallelization which would decrease computing time.

Considering again the predictions of pressures and heating rates in Figs. 8–17, the agreement with data obtained by the new approximate technique is at least comparable and in some cases better than that of the more exact CFL3D code. Similar agreement was also found in circumferential data comparisons that are not shown in this paper. However, the advantage of the approximate method is that, for similar accuracy, model development and analysis times (both user and CPU) are significantly smaller than the more complex CFD codes.

Concluding Remarks

Previous three-dimensional heating codes that use approximate techniques such as the axisymmetric analog method also use Modified Newtonian body pressures. An extension to these codes has been developed that incorporates a new Embedded Newtonian pressure equation into the calculations. This approach accounts for the effects of embedded shock waves and entropy layer swallowing on the flowfield. The enhanced capability allows more accurate computation of pressures and heating rates over the increasingly complex hypersonic vehicle configurations of current interest. Although approximate in nature, the results obtained by the current method compare favorably to available experimental data and contemporary CFD codes.

One significant concern about the approximate as well as CFD techniques is their dependence on accurate modeling of the vehicle geometry, including surface slope and curvature. The ASTUD and QUICK geometry definition methods were found to produce acceptable models of vehicle configurations with complex surface characteristics such as discontinuities. These techniques represent surface discontinuities better than other methods such as spline fits. This capability is needed for the prediction of embedded shocks in the flowfield.

Major advantages of the approximate method in relation to more exact CFD techniques include significant reductions in CPU time to calculate solutions. Also, there is much less user interaction required for the approximate method beyond the initial vehicle geometry definition. Substantial time investments are often required of the user of the more exact codes to address issues such as grid refinement and shock fitting. These advantages make the approximate method a competitive tool in a preliminary design environment.

Acknowledgments

This research was supported under Contract F33615-87-C-3402 with McDonnell Douglas Corporation as a part of the hypersonic thermal analysis for aircraft transparencies program performed by McDonnell Aircraft Company for the Wright Research and Development Center. The U.S. Air Force technical monitor was Charles A. Babish III. The first author was also supported under a National Defense Science and Engineering Graduate fellowship sponsored by the Air Force Office of Scientific Research, Bolling Air Force Base, Washington, DC.

References

[1]Cooke, J. C., "An Axially Symmetric Analogue for General Three-Dimensional Boundary Layers," British Ministry of Aviation, Aeronautical Research Council TR, R&M 3200, London, June 1961.

[2]DeJarnette, F. R., "Calculation of Inviscid Surface Streamlines and Heat Transfer on Shuttle Type Configurations, Part I—Description of Basic Method," NASA CR-111921, Aug. 1971.

[3]DeJarnette, F. R., and Hamilton, H. H., "Aerodynamic Heating on Three-Dimensional Bodies Including the Effects of Entropy Layer Swallowing," *Journal of Spacecraft and Rockets,* Vol. 12, No. 1, 1975, pp. 5–12.

[4]Fivel, H. J., "Numerical Flow Field Program for Aerodynamic Heating Analysis Volumes I and II," Air Force Flight Dynamics Lab., Rept. AFFDL-TR-79-3128, Wright-Patterson AFB, OH, Dec. 1979.

[5]Varner, M. O., Adams, J. C., Boylan, D. E., Gwinn, A. F., LeMaster, R. A., Martindale, W. R., and Nopratvarakorn, V., "Specific Thermal Analyzer Program for High-Temperature Resistant Transparencies for High-Speed Aircraft (STAPAT), Vol. I, Methodology," Air Force Wright Aeronautical Lab., Rept. AFWAL-TR-84-3086, AD B090 894L, Wright-Patterson AFB, OH, Oct. 1984.

[6]Boman, B. L., "Hypersonic Thermal Analysis For Aircraft Transparencies, Vol. I—STAPAT II Description," Wright Research and Development Center, Rept. WRDC-TR-90-3053, Wright-Patterson AFB, OH, Sept. 1990.

[7]Cassel, L. A., and Jarrett, T. W., "Hypersonic Flow over Small Span Flaps in a Thick Turbulent Boundary Layer," *Aerothermodynamics and Planetary Entry,* edited by A. L. Crosbie, Vol. 77, Progress in Astronautics and Aeronautics, AIAA, New York, 1981, pp. 137–166.

[8]Kuntz, D. W., Polansky, G. F., and Buffington, R. J., "A Comparison of Predicted and Measured Aeroheating on a Reentry Vehicle Flap Geometry," AIAA Paper 87-0517, Jan. 1987.

[9]Cheatwood, F. M., DeJarnette, F. R., and Hamilton, H. H., "Interactive Approach to Surface Fitting Complex Geometries for Flowfield Applications," *Journal of Spacecraft and Rockets,* Vol. 26, No. 1, 1989, pp. 31–38.

[10]Daywitt, J. E., "Geometry Input and Flow Field Output Processors for a Parabolized Navier-Stokes Program, Vols. I–III," Air Force Wright Aeronautical Lab., Rept. AFWAL-TR-83-3112, Wright-Patterson AFB, OH, Nov. 1983.

[11]Bapu, P. T., Orr, C. E., and Stump, W. J., "Interactive Geometry Input Processors for a Parabolized Navier-Stokes Program, Vols. I–III," Air Force Wright Aeronautical Laboratories, Rept. AFWAL-TR-87-3113, Wright-Patterson AFB, OH, Feb. 1988.

[12]Cohen, N. B., "Boundary-Layer Similar Solutions and Correlation Equations for Laminar Heat-Transfer Distribution in Equilibrium Air at Velocities Up to 41,100 Feet Per Second," NASA TR R-118, 1961.

[13]Reshotko, E., and Tucker, M., "Approximate Calculations of the Compressible Turbulent Boundary Layer with Heat Transfer and Arbitrary Pressure Gradient," NACA TN 4154, Dec. 1957.

[14]Spalding, D. B., and Chi, S. W., "The Drag of a Compressible Turbulent Boundary Layer on a Smooth Flat Plate With and Without Heat Transfer," *Journal of Fluid Mechanics,* Vol. 18, Pt. 1, Jan. 1964, pp. 117–143.

[15]Maslen, S. H., "Inviscid Hypersonic Flow Past Smooth Symmetric Bodies," *AIAA Journal,* Vol. 5, No. 6, 1964, pp. 1055–1061.

[16]Anon., "Equations, Tables, and Charts for Compressible Flow," NACA TR-1135, 1953.

[17]Kuethe, A. M., and Chow, C., *Foundations of Aerodynamics,* 4th ed., Wiley, New York, 1986, pp. 232–235.

[18]Landrum, D. B., and DeJarnette, F. R., "Modifications to the STAHET Aeroheating Program," Mars Mission Research Center, Rept. MMRC 90-1, North Carolina State Univ., Raleigh, NC, March 1990.

[19]Wilhite, A. W., "Optimum Wing Sizing of a Single-Stage-to-Orbit Vehicle," *Journal of Spacecraft and Rockets,* Vol. 20, No. 2, 1983, pp. 115–121.

[20]Ericsson, L. E., "Unsteady Embedded Newtonian Flow," *Astronautica Acta,* Vol. 18, No. 5, 1973, pp. 309–330.

[21]Anon., "National Aerospace Plane Generic Option 2: Experimental Database/CFD Code Validation," Final Rept., Contract F33657-86-C-2126, McDonnell Douglas, St. Louis, MO, Sept. 1988.

[22]Boman, B., and Babish, C., "Application of the STAPAT II Code to Hypersonic Vehicle Aerothermodynamics," AIAA Paper 91-5035, Dec. 1991.

[23]Thompson, R., and Gnoffo, P., "Application of the LAURA Code for Slender Vehicle Aerothermodynamics," AIAA Paper 90-1714, June 1990.

[24]Richardson, P., Parlette, E., Morrison, J., Switzer, G. Dilley, A., and Eppard, W., "Heat Transfer and Pressure Comparisons Between Computation and Wind Tunnel for Research Hypersonic Aircraft," AIAA Paper 89-0028, Jan. 1989.

Ernest V. Zoby
Associate Editor